J Fluoresc (2015) 25:137–145
DOI 10.1007/s10895-014-1490-0

ORIGINAL PAPER

Photoinduced Electron Transfer from Phenanthrimidazole to Magnetic Nanoparticles

J. Jayabharathi · A. Arunpandiyan · V. Thanikachalam · P. Ramanathan

Received: 30 September 2014 / Accepted: 2 December 2014 / Published online: 17 January 2015

Abstract The dynamics of photoinduced electron injection from (E)-1-(4-methoxyphenyl)-2-styryl-1H-phenanthro [9,10-d]imidazole (MPSPI) synthesised using nano TiO_2 as catalyst to Fe_2O_3 nanocrystal has been studied by FT-IR, absorption, fluorescence and lifetime spectroscopic methods. The binding between nanoparticle and MPSPI is confirmed by binding constant and binding site. The distance between MPSPI and nanoparticle as well as the critical energy transfer distance has been obtained. The free energy change (ΔG_{et}) for electron injection has also been deduced.

Keyword Phenanthrimidazole · Fe_2O_3 nanocrystal · Electron transfer

Introduction

Arylimidazoles play important role in materials science and medicinal chemistry due to their optoelectronic properties and high thermal stabilities [1–7]. Substituted imidazoles are extensively used as glucagon receptors [8], CB1 cannabinoid receptor antagonists [9] and modulators of P-glycoprotein (P-gp)-mediated multidrug resistance (MDR) [10], antibacterial [11], anti-allergic [12], analgesic [13], antitumor [14] and also as pesticides [15]. Many of the reported synthetic protocols for imidazoles [16–31] suffer from more disadvantages such as use of toxic organic solvents, acidic conditions, complex work-up, purification, side reactions, low yield and use of hazardous and expensive reagents. Thus the development of a new catalyst is essential to overcome these shortcomings and to fulfill the criteria of a milder reaction conditions, higher yield and reusability of catalyst. Titanium dioxide find widespread industrial applications [32–36] and its utility has been extended to the photodegradation of pesticides [37] and carcinogenic dyes [38, 39]. From a synthetic point of view, titanium dioxide has been as a green, inexpensive, mild and recyclable heterogeneous Lewis acid potential catalyst in certain organic transformations like Beckmann rearrangement [40], Fridel-Crafts acylation [41], Biginelli condensation [42] and also the synthesis of dihydropyrazines [43], piperazines [44], quinoxalines [45] and photocatalytic oxidation of amines [46].

Nano sized iron oxide particulates have emerged as versatile materials for different applications due to their, magnetic, electronic, photonic and optical properties. The structure-function relationship of these nano particles have been intensively studied because of the applications in magnetic storage, gas sensing, biomedical and catalysis applications [47–56]. Out of various phases of iron oxide nano particle recently great interest has been devoted towards to the synthesis of α-phase of iron oxide nano particles (α-Fe_2O_3, hematite). These are of technological interest for the use in photoelectrochemical (PEC) water splitting reaction for the production of hydrogen [57]. Hematite is the inexpensive material of interest for PEC application due to its suitable band gap 2.2 eV, valence band edge position, earth abundance and environmentally benign nature [58]. Some researchers have reported the specific interaction between nanoparticles and protein as well as other biomolecules [59–63]. There are many reports on the photoinduced electron transfer from organic molecule to nanoparticle semiconductors [64–71].

J. Jayabharathi (✉) · A. Arunpandiyan · V. Thanikachalam · P. Ramanathan
Department of Chemistry, Annamalai University, Annamalainagar, Chidambaram 608002, Tamilnadu, India
e-mail: jtchalam2005@yahoo.co.in

Materials and Methods

Measurements

XRD patterns were recorded for the centrifuged and dried samples using X–ray Rigaku diffractometer with Cu K_α source (30 kV, 100 mA), at a scan speed of 3.0000 deg/min, step width of 0.1000 deg, in a 2θ range of 20–80 . The energy dispersive X-ray (EDS) spectra of the nanosemiconductors were recorded with a JEOL JSM-5610 scanning electron microscope (SEM) equipped with back electron (BE) detector and EDX. The sample was placed on an adhesive carbon slice supported on copper stubs and coated with 10 nm thick gold using JEOL JFC- 1600 auto fine coater prior to measurement.

The ^{1}H and ^{13}C NMR spectra at 400 and 100 MHz, respectively were obtained at room temperature using a Bruker 400 MHz NMR spectrometer (Bruker biospin, California, USA). The mass spectra were obtained using a Thermo Fischer LC-Mass spectrometer in fast atom bombardment (FAB) mode (Thermo, France). The UV–vis and photoluminescence spectra were recorded with Perkin Elmer Lambda 35 UV–vis spectrophotometer and PerkinElmer LS55 fluorescence spectrometer, respectively.

The lifetime measurements were carried out with a nanosecond time correlated single photon counting (TCSPC) spectrometer Horiba Fluorocube-01-NL lifetime system with Nano LED (pulsed diode exCitation source) as the excitation source and TBX-PS as detector. The quantum yields were measured by comparing the emission intensities of a standard sample and the unknown sample [72–74] using the formula, $\Phi_{unk}=\Phi_{std}\left(\frac{I_{unk}}{I_{std}}\right)\left(\frac{A_{std}}{A_{unk}}\right)\left(\frac{\eta_{unk}}{\eta_{std}}\right)^2$, Φ_{unk} and Φ_{std} are the quantum yield of the sample and the standard, respectively; I_{unk} and I_{std} are the integrated emission intensities of the sample and the standard, respectively. A_{unk} and A_{std} are the absorbance of the sample and the standard at the excitation wavelength, respectively. η_{unk} and η_{std} are the refractive index of the sample and standard solutions, respectively. The cyclic voltammetry analyses were performed with CHI electrochemical analyzer 604C (CHI electrochemical analyzer, USA) at a scan rate of 100 mV s^{-1} using 0.1 M tetra-(*n*-butyl)-ammonium hexafluorophosphate as supporting electrolyte with Ag/Ag^{+} (0.01 M $AgNO_3$) as the reference electrode and Pt electrode as the working electrode, standardized for the redox couple ferricinium/ferrocene. All solutions were purged with a nitrogen stream for 10 min before measurement. Thermal analysis of the phenanthrimidazoles was made with NETZSCH-Geratebau Gmbh thermal analysis STA 409 PCO. The differential scanning calorimetric (DSC) and thermogravimetric analyses (TGA) were made under nitrogen atmosphere (100 mL min^{-1}). The sensitivity of the instrument was set at 0.01 μg and the sample (10 mg) was heated from 30 to 700 ° C at the rate of 10 or 15 or 20 K min^{-1}. DFT calculations were performed with Gaussian-03 [75] package.

Synthesis of (E)-1-(4-Methoxyphenyl) -2-Styryl-1H-Phenanthro [9,10-d]Imidazole (MPSPI)

A mixture of chinnamaldehyde (1 mmol), phenanthrene-9,10-dione (1 mmol), 4-methoxyaniline (1 mmol) and ammonium acetate (1 mmol) with TiO_2 (1 mol%) as catalyst was stirred at 120 °C in an ice bath with continuous stirring with a bar magnet. The progress of the reaction was monitored by TLC (Scheme 1). After completion of the reaction, 10 ml of ethyl acetate was added to the reaction mixture and shaken well to dissolve the organic components and the mass filtered to separate out TiO_2 and the residue was washed with ethyl acetate. The solid residue of TiO_2 was further washed with hot acetone and then dried up. The product was purified by column chromatography using benzene: ethyl acetate (9:1) as the eluent. Yield: 79 %, M.p. 212 °C, Anal. calcd. for $C_{30}H_{22}N_2O$: C, 84.48; H, 5.20; N, 6.57. Found: C, 84.46; H, 5.19; N, 6.56. ^{1}H NMR (400 MHz, DMSO): δ 3.917 (s, 3H), 7.97 (d, J=8.8Hz, 1H), 8.09 (d, J=8.4Hz, 1H), 8.23 (d, J= 7.2Hz, 2H), 8.34 (d, J=8.8Hz, 1H), 8.96 (d, J=9.2Hz, 1H), 7.41–7.54 (m, 8H), 7.67–7.87 (m, 4H). ^{13}C NMR (400 MHz, DMSO): δ 55.49, 105.55, 113.81, 118.85, 120.05, 120.60, 122.19, 122.30, 124.11, 126.57, 126.82, 127.74, 127.86, 127.90, 128.04, 128.28, 128.75, 128.96, 129.11, 129.33, 130.53, 131.47, 134.92, 135.09, 135.90, 138.08, 138.75, 143.51, 153.59, 157.22, 161.89. MS: m/z 426 [M+].

Results and Discussion

Characterisation of Fe_2O_3 Nanocrystal

Figure 1 display the powder diffraction pattern of the imidazole bound magnetic nanoparticles. The recorded XRD is in agreement with that of maghemite cubic Fe_2O_3 with unit cell length as 0.8352 nm. The peaks at 30.2, 35.7, 43.3, 53.7, 57.3 and 62.9° correspond to 220, 311, 400, 422, 511 and 440-planes, respectively [JCPDS card no. 39–1346]. Figure 1 (XRD 15–80°) presents the XRD of imidazole bound magnetic nanoparticles. The mean crystallite size (*L*) of the imidazole bound nanoparticles is 30.3 nm and the calculated surface area is 50.58 m^2/g.

Absorption of MPSPI – Nanocrystalline Fe_2O_3

Figure 2 display the absorption spectra of MPSPI in presence of Fe_2O_3 nanocrystals dispersed at different loading and also in their absence. Nano Fe_2O_3 enhance the absorbance of MPSPI remarkably without shifting its absorption maximum

Scheme 1 Possible mechanism for catalytic synthesis of phenanthrimidazole

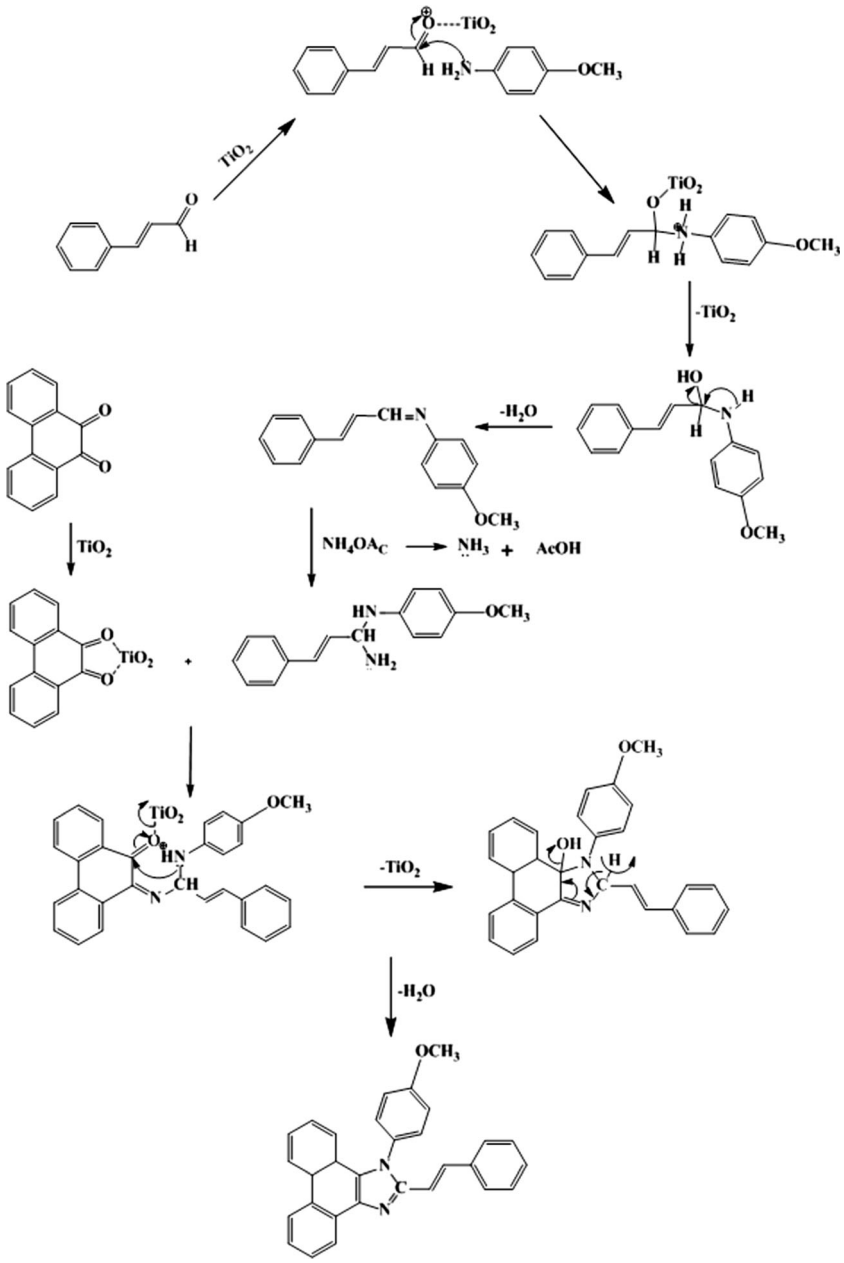

at 258 nm. This indicates that the semiconductor nanocrystals do not modify the excitation process of the ligand. The enhanced absorption at 258 nm observed with the dispersed nanoparticles are due to adsorption of the MPSPI on surface of nanocrystals. This is because of effective transfer of electron from the excited state of the MPSPI to the conduction band of the semiconductor nanoparticles.

FT-IR Characteristics of MPSPI –Nanocrystalline Fe_2O_3

The FT-IR spectrum of MPSPI and also that of MPSPI adsorbed on the nanocrystals are recorded. The spectrum of MPSPI shows the > *C*=N stretching vibration at 1602 cm^{-1}. This band is shifted to 1632 cm^{-1} allowed to adsorb on the nanocrystals. These observations show that the MPSPI is bound to the surface of nanoparticles.

Fluorescence Quenching Characteristics

The fluorescence quenching technique is applied to study the interaction between nanomaterials and MPSPI, to infer the association and also the electron transfer between them as indicated in Scheme 2. Addition of nanoparticles to the solution of MPSPI resulted in the quenching of its fluorescence.

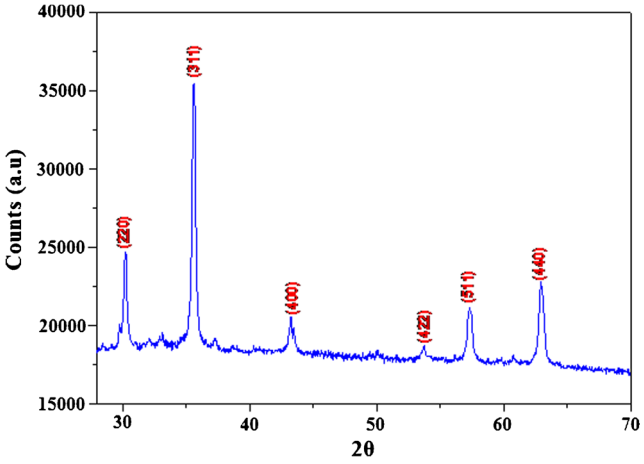

Fig. 1 Powder X-ray diffraction (XRD) pattern of MPSPI

Figure 3 displays the effect of increasing concentration of nanoparticles on the fluorescence spectrum of MPSPI. This quenching behavior is similar to the studies reported earlier [76]. The apparent association constants (K_{app}) have been obtained from the fluorescence quenching data using the following equation

$$1/(F_0 - F) = 1/(F_0 - F) + 1/K_{app}(F_0\text{-}F)\ [\text{nanoparticles}] \quad (1)$$

where K_{app} is the apparent association constant, F_0 is the initial fluorescence intensity of MPSPI, F is the fluorescence intensity of MPSPI adsorbed on nanoparticles. A good linear relationship between $1/(F_0$ and F) and the reciprocal concentration of nanoparticles is seen. From the slope, the values of K_{app} have been assessed for MPSPI – nano Fe_2O_3 as 3.68×10^7.

The fluorescence quenching behavior is usually described by Stern–Volmer relation $I_0/I = 1 + K_{SV}$ [Q]. Here, I_0 and I are the fluorescence intensities in the absence and presence of quencher, K_{SV} is the Stern–Volmer constant related to the bimolecular quenching rate constant and Q is the quencher. Figure 4 presents the Stern-Volmer plot. The ability of the excited state MPSPI to inject its electrons into the conduction band of nanoparticles is determined from the energy difference between the conduction band of nanoparticles and excited state oxidation potential of MPSPI.

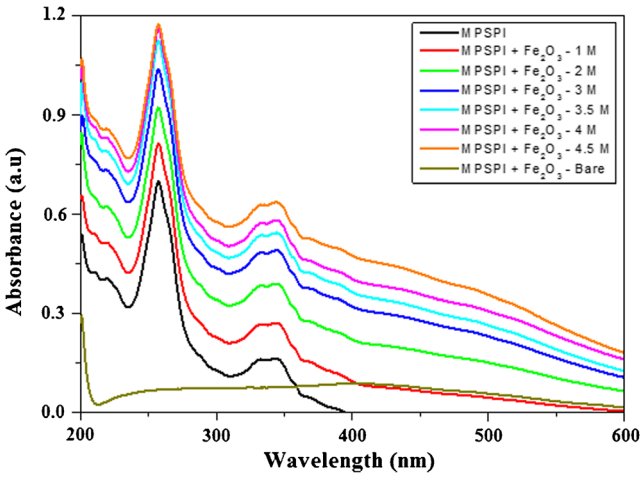

Fig. 2 Absorption spectra of MPSPI in presence and absence of Fe_2O_3 nanocrystal with various concentrations

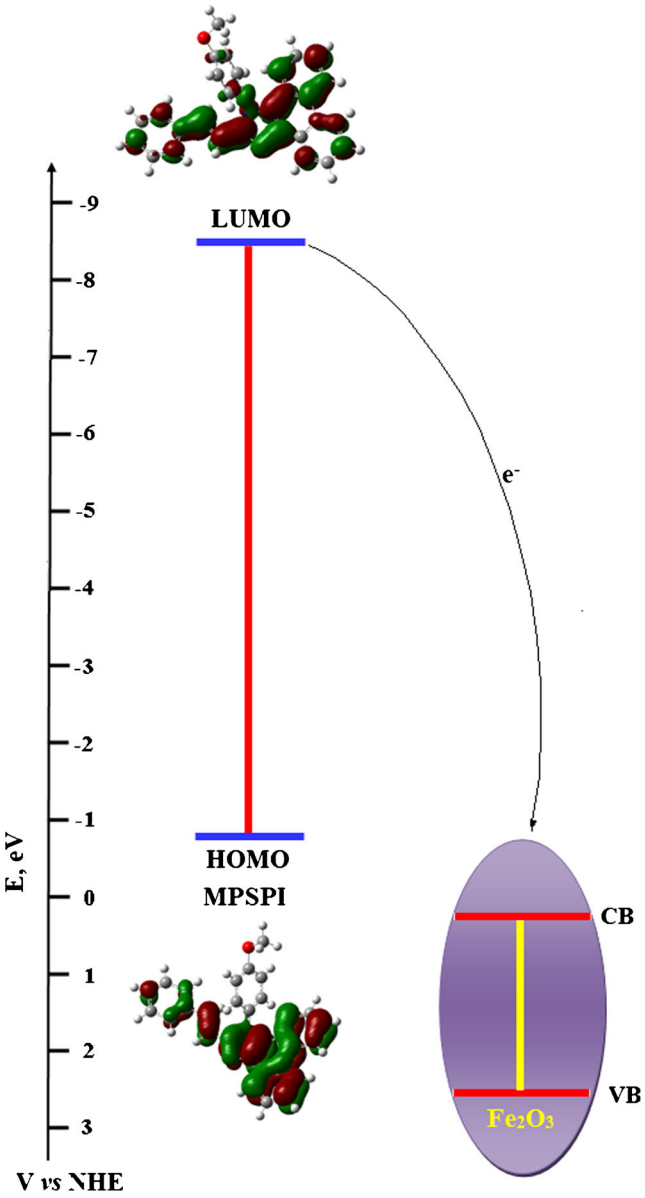

Scheme 2 Schematic diagram describing the electron-donating energy level of MPSPI

Energetics

From the onset oxidation potential (E_{ox}) and the onset reduction potential (E_{red}) of the benzimidazole, HOMO and LUMO energy levels have been calculated according to the equations: HOMO$=-e(E_{ox}+4.71)$ (eV), LUMO$=-e(E_{red}+4.71)$ (eV),

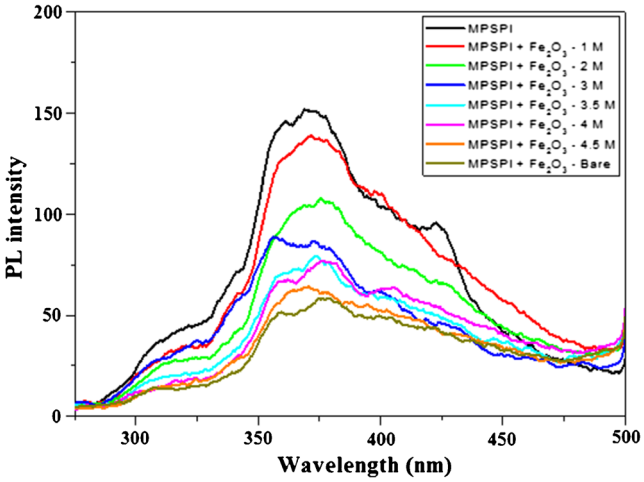

Fig. 3 Fluorescence spectra of MPSPI in the presence and absence of Fe_2O_3 nanocrystal with various concentrations

HOMO-LUMO energies of phenanthrimidazole are also calculated theoretically. The theoretically calculated energies are in good agreement with the experimental values. On the basis of the relative positions of phenanthrimidazole derivative and Fe_2O_3 energy levels shown in Scheme 2, the electron injection would be thermodynamically allowed from the excited singlet of the phenanthrimidazole derivative to the conduction band of nanocrystalline Fe_2O_3.

From HOMO-LUMO analysis of MPSPI, the oxidation potential of excited singlet state MPSPI is obtained as −1.84 V (vs. NHE), using the equation, $E_{s*/s+}=E_{s/s+}-E_s$. Here, $E_{s/s+}$ is the oxidation potential of 0.20 V (vs. NHE) and *E*s is the excited state energy, 2.04 eV. The excited state energy of the MPSPI is calculated from the fluorescence maximum based on the reported method [77]. The energy level of the conduction band of semiconductor nanoparticles is shown in Scheme 2 [78]. It suggests that the electron transfer from excited state MPSPI to the conduction band of nanoparticulate semiconductors is energetically favourable.

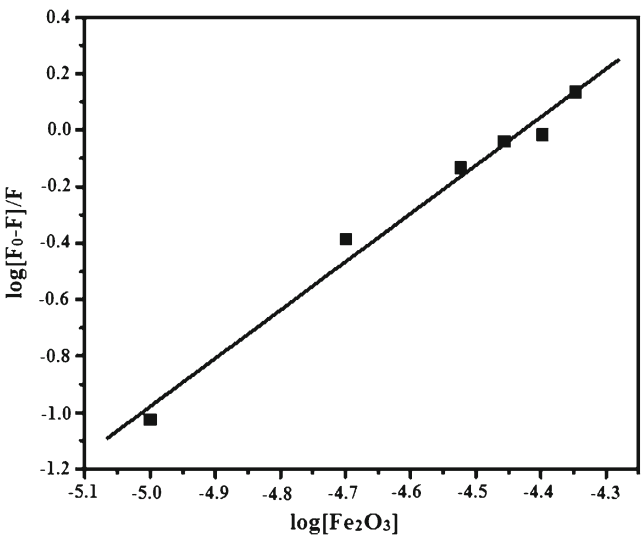

Fig. 4 Stern-Volmer plot of MPSPI with Fe_2O_3 nanocrystal

Binding Constant and Number of Binding Sites

Static quenching arises from the formation of complex between fluorophore and the quencher and the binding constants (*K*) have been calculated by employing the equation

$$log\ [(F_0 - F)/F] = log\ K + nlog\ [Q] \quad (2)$$

where K is the binding constant of nanoparticles with FPPBI and the calculated value of binding constant value 372.24×10^7 and the number of binding site (n) is 1.20.

Electron Transfer Between MPSPI – Nanocrystalline Fe_2O_3

The decrease in fluorescence intensity is attributed to electron transfer between MPSPI and the nanoparticles in the case of semiconductors. The excited state energy of the MPSPI is larger than the conductance band energy levels of nanosemiconductors [79]. This makes possible the energy transfer from the excited state of MPSPI to the nanoparticles. The energy transfer efficiency (*E*) is calculated using the equation, $E=1-(I/I_0)$, as 0.59 (Fe_2O_3). Here, I is the emission intensity of donor in the presence of acceptor and I_0 is the emission intensity of the donor alone. From the above results it is clear that, in presence of nanoparticles, the fluorescence intensity of MPSPI is reduced (from I_0 to I) by energy transfer to nanoparticles.

According to Forster's non-radiative energy transfer theory [80], the energy transfer efficiency (E) is related not only to the distance between the acceptor and donor (r_0), but also to the critical energy transfer distance (R_0). That is, $E=R^6_0/(R^6_0+r^6_0)$, where, R_0 is the critical distance when the transfer efficiency is 50 %. $R^6_0=8.8\times10^{-25}K^2N^{-4}\ \varphi\ J$, where, K^2 is the spatial orientation factor of the dipole, N is the refractive index of the medium, φ is the fluorescence quantum yield of the donor and J is the overlap integral of the fluorescence emission spectrum of the donor and the absorption spectrum of the acceptor. The value of J can be calculated by using the equation, $J=\int F(\lambda)\varepsilon(\lambda)\lambda^4 d\lambda / F(\lambda)d\lambda$, where, F(λ) is the fluorescence intensity of the donor, ε(λ) is molar absorptivity of the acceptor. The parameter J can be evaluated by integrating the spectral parameters as 9.76×10^{-12} cm^3 L mol^{-1}. Under these experimental conditions, the value of R_0 is found to be about 0.69 nm for the nanocrystals; the values of K^2 (=2/3) and N (=1.3467) used are from the literature [81] and the φ value is from the present study. Obviously, the calculated value of R_0 is in the range of maximal critical distance. This is in accordance with the conditions of Forster's non-radiative energy transfer theory [82, 83], indicating the static quenching

Table 1 Bi-Exponential fitting parameter for fluorescence decay

Compound	τ1	τ2	α_1	α_2	x^2	τ_{avg}	k_r	k_{nr}
MPSPI	2.3764×10^{-9}	9.0258×10^{-9}	4.0317×10^{-2} (77.84)	3.0221×10^{-3} (22.16)	1.04	2.84	0.17	0.18
MPSPI - Fe_2O_3	2.2007×10^{-9}	1.1364×10^{-8}	3.6920×10^{-2} (74.46)	2.4599×10^{-3} (25.60)	1.12	2.77	0.18	0.18

values within the parenthesis corresponds to relative amplitude

interaction between nanoparticles and MPSPI. The value of r_0 (0.91 nm) is less than 8 nm which is larger than that of R_0 in the present study also reveals the operation of static-type of quenching mechanism [84].

Free Energy Change (Δ_{Get}) for Electron Transfer Processes

The thermodynamic feasibility of excited state electron transfer reaction has been confirmed by the calculation of free energy change by employing the well known Rehm-Weller expression [85].

$$G_{et} = E^{1/2}{}_{(ox)} - E^{1/2}{}_{(red)} - E_s + C \quad (3)$$

where, $E^{1/2}{}_{(ox)}$ is the oxidation potential of MPSPI, $E^{1/2}{}_{(red)}$ is the reduction potential of nanoparticles, that is, the conduction band potential of nanoparticles, Es is the excited state energy of MPSPI and C is the coulombic term. Since one of the species is neutral and the solvent used is polar in nature, the coulombic term in the above expression can be neglected [86]. The values of ΔG_{et} are calculated as −3.32 eV. The high negative values indicate the thermodynamic feasibility of the electron transfer process [87].

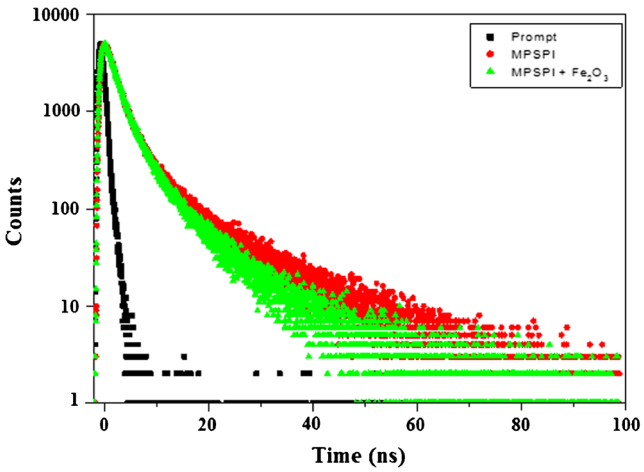

Fig. 5 Fluorescence lifetime spectra of MPSPI in presence and absence of Fe_2O_3 nanocrystal

Fluorescence lifetime measurements

An alternative way to rationalize the binding behaviour in the present study is by considering the fluorescence lifetime of FPPBI with nanoparticles. The experimental decay curves were fit to a bi exponentials, $f(t)=\alpha_1 \exp(-t/\tau_1)+\alpha_2 \exp(-t/\tau_2)$, where α_1 and τ_1 are respectively, the pre-exponential factor and lifetime of the various excited states involved. This model is based on the assumption that one, two or three fluorescent substances are present in the solution. The fluorescence decay curves of all nanoparticles with MPSPI were recorded in ethanol. Laser excitation was set at 270 nm and the fluorescence signal was measured at emission wavelength of individual compound. The fluorescence decay was fitted with a biexponential function and the decay time, radiative (k_r), non-radiative (k_{nr}) constants and energy transfer rate constants (k_{et}) are presented in Table 1. Fe_2O_3 nanocrystals bound to change the fluorescence lifetime. The results can be visualized as shown in Fig. 5. Examination of rate constant of energy transfer shows that energy transfer is more with Fe_2O_3 nanocrystals which are strongly bound to the ligand. The strongly bound nanocrystal Fe_2O_3 displays a large electron transfer rate. That is the binding constant and the rate of electron transfer is related.

Conclusions

Fluorophore (E)-1-(4-methoxyphenyl)-2-styryl-1H-phenanthro [9,10-d]imidazole (MPSPI) is adsorbed on the surface of semiconductor nanoparticles through azomethine nitrogen. The conduction band energy positions determine the electron transfer from excited state MPSPI to the nanoparticles. The distance between the MPSPI and nanoparticles, deduced on the basis of Forester's non-radiation energy transfer theory. The negative ΔG_{et} values for all nanoparticles reveal that the electron transfer process is thermodynamically favorable. Electron transfer from MPSPI to nanoparticles is explained in detail.

Acknowledgments One of the authors Prof. J. Jayabharathi is thankful to DST (No. SR/S1/IC-73/2010), DRDO (NRB-213/MAT/10-11), UGC (F. No. 36-21/2008 (SR)) and CSIR (NO 3732/NS-EMRII) for providing funds to this research study.

References

1. Hush NS (1985) Distance dependence of electron transfer rates. Coord Chem Rev 64:135–157
2. Marcus RA (1989) Relation between charge transfer absorption and fluorescence spectra and the inverted region. J Phys Chem 93: 3078–3086
3. Gould IR, Young RH, Moody RE, Farid S (1991) Contact and solvent-separated geminate radical ion pairs in electron-transfer photochemistry. J Phys Chem 95:2068–2080
4. Gould IR, Noukakis D, Gomez-Jahn L, Young RH, Goodman JL, Farid S (1993) Radiative and nonradiative electron transfer in contact radical-ion pairs. J Chem Phys 176:439–456
5. Cortes J, Heitele H, Jortner J (1994) Band-shape analysis of the charge-transfer fluorescence in barrelene-based electron donor-acceptor compounds. J Phys Chem 98:2527–2536
6. Mulliken RS, Person WB (1969) Molecular complexes: a lecture and reprint volume. Weinheim, VCH
7. Nelson J, Haque SA, Klug DR, Durrant JR (2001) Trap-limited recombination in dye-sensitized nanocrystalline metal oxide electrodes. Phys Rev B 63:205321
8. deLaszlo SE, Hacker C, Li B, Kim D, Maccoss M, Mantle N, Pivnichny JV, Colwell L, Koch GE, Cascieri MA, Hagmann WK (1999) Potent, orally absorbed glucagon receptor antagonists. Bioorg Med Chem Lett 9:641–646
9. Eyers PA, Craxton M, Morrice N, Cohen P, Goedert M (1998) Conversion of SB 203580-insensitive MAP kinase family members to drug-sensitive forms by a single amino-acid substitution. Chem Biol 5:321–328
10. Newman MJ, Rodarte JC, Benbatoul KD, Romano SJ, Zhang C, Krane S, Moran EJ, Uyeda RT, Dixon R, Guns ES, Mayer LD (2000) Cancer Res 60:2964–2972
11. Antolini M, Bozzoli A, Ghiron C, Kennedy G, Rossi T, Ursini A (1999) Analogues of 4,5-bis (3,5-dichlorophenyl)-2-trifluoromethyl-1H-imidazole as potential antibacterial agents. Bioorg Med Chem Lett 9:1023–1028
12. Black JW, Durant GJ, Emmett JC, Ganellin CR (1974) Sulphur-methylene isosterism in the developent of metiamide, a new histamine H_2-receptor antagonist. Nature 248:65–67
13. Uçucu Ü, Karaburun NG, Işikdağ İ (2001) Synthesis and analgesic activity of some 1-benzyl-2-substituted-4,5-diphenyl-1H-imidazole derivatives. Il Farmacol 56:285–290
14. Wang L, Woods KW, Li Q, Barr KJ, McCroskey RW, Hannick SM, Gherke L, Credo RB, Hui YH, Marsh K, Warner R, Lee JY, Zielinski-Mozng N, Frost D, Rosenberg SH, Sham HL (2002) Potent, orally active heterocycle-based combretastatin A-4 analogues: synthesis, structure-activity relationship, pharmacokinetics, and in vivo antitumor activity evaluation. J Med Chem 45:1697–1711
15. Maier T, Schmierer R, Bauer K, Bieringer H, Buerstell H, Sachse B (1989) US Patent 4820335, Chem. Abstr. 111, 1949w.
16. Siddiqui SA, Narkhede UC, Palimkar SS, Daniel T, Lahoti RJ, Srinivasan KV (2005) Room temperature ionic liquid promoted improved and rapid synthesis of 2,4,5-triaryl imidazoles from aryl aldehydes and 1,2-diketones or α-hydroxyketone. Tetrahedron 61: 3539–3546
17. Heravi MM, Zakeri M, Karimi N, Saeedi M, Oskooie HA, Hosieni NT (2010) Acidic ionic liquid [(CH2) 4SO3HMIM] [HSO4]: a green media for the simple and straightforward synthesis of 2, 4, 5-trisubstituted imidazoles. Synth Commun 40:1998–2006
18. Wang J, Mason R, VanDerveer D, Feng K, Bu XR (2003) Convenient preparation of a novel class of imidazo [1,5-a]pyridines: decisive role by ammonium acetate in chemoselectivity. J Org Chem 68: 5415–5418
19. Sarshar S, Siev D, Mjalli MM (1996) Imidazole libraries on solid support. Tetrahedron Lett 37:835–838
20. Gallagher TF, Seibel GL, Kassis S, Laydon JT, Blumenthal MJ, Lee JC, Lee D, Boehm JC, Fier-Thompson SM, Abt JW, Soreson ME, Smietana JM, Hall RF, Garigipati RS, Bender PE, Erhard KF, Krog AJ, Hofmann GA, Sheldrake PL, McDonnell PC, Kumar S, Young PR, Adams JL (1997) Regulation of stress-induced cytokine production by pyridinylimidazoles; inhibition of CSBP kinase. Bioorg Med Chem 5:49–64
21. Shaabani A, Rahmati A (2006) Silica sulfuric acid as an efficient and recoverable catalyst for the synthesis of trisubstituted imidazoles. J Mol Catal A Chem 249:246–248
22. Kantevari S, Vuppalapati SVN, Biradar DO, Nagarapu L (2007) Highly efficient, one-pot, solvent-free synthesis of tetrasubstituted imidazoles using HClO < sub > 4</sub > −SiO < sub > 2</sub > as novel heterogeneous catalyst. J Mol Catal A Chem 266:109–113
23. Kidwai M, Mothsra P, Babsal V, Goyal R (2006) Efficient elemental iodine catalyzed one-pot synthesis of 2,4,5-Triarylimidazoles. Monatsh Chem 137:1189–1194
24. Wang LM, Wang YH, Tian H, Yao YF, Shao JH, Liu B (2006) Ytterbium triflate as an efficient catalyst for one-pot synthesis of substituted imidazoles through three-component condensation of benzil, aldehydes and ammonium acetate. J Fluor Chem 127: 1570–1573
25. Sharma GVM, Jyothi Y, Lakshmi PS (2006) Efficient room-temperature synthesis of triand tetrasubstituted imidazoles catalyzed by $ZrCl_4$. Synth Commun 36:2991–3000
26. Balalaie S, Arabanian A (2000) One-pot synthesis of tetrasubstituted imidazoles catalyzed by zeolite HY and silica gel under microwave irradiation. Green Chem 2:274–276
27. Heravi MM, Bakhtiari K, Oskooie HA, Taheri S (2007) Synthesis of 2,4,5-triaryl-imidazoles catalyzed by NiCl 2·6H 2O under heterogeneous system. J Mol Catal A Chem 263:279–281
28. Sivakumar K, Kathirvel A, Lalitha A (2010) Simple and efficient method for the synthesis of highly substituted imidazoles using zeolite-supported reagents. Tetrahedron Lett 51:3018–3021
29. Hayes JF, Mitchell MB, Wicks C (1994) A novel synthesis of 2,4,5-triarylimidazoles. Heterocycles 38:575–585
30. Revesz L, Bonne F, Makavou P (1998) Vicinal bromostannanes as novel building blocks for the preparation of di- and trisubstituted imidazoles. Tetrahedron Lett 39:5171–5174
31. Liverton NJ, Butcher JW, Claiborne CF, Claremon DA, Libby BE, Nguyen KT, Pitzenberger SM, Selnick HG, Smith GR, Tebben A, Vacca JP, Varga SL, Agarwal L, Dancheck K, Forsyth AJ, Fletcher DS, Frantz B, Hanlon WA, Harper CF, Hofsess SJ, Kostura M, Lin J, Luell S, O'Neill EA, Orevillo CJ, Pang M, Parsons J, Rolando A, Sahly Y, Visco DM, O'Keefe SJ (1999) Design and synthesis of potent, selective, and orally bioavailable tetrasubstituted imidazole inhibitors of p38 mitogen-activated protein kinase. J Med Chem 42: 2180–2190
32. Diebold U (2003) The surface science of titanium dioxide. Surf Sci Rep 48:53–229
33. Tryk DA, Fujishima A, Honda K (2000) Recent topics in photoelectrochemistry: achievements and future prospects. Electrochim Acta 45:2363–2376
34. Phillips LG, Barbano DM (1997) The influence of Fat substitutes based on protein and titanium dioxide on the sensory properties of lowfat milks[1]. J Dairy Sci 80:2726–2731
35. Hewitt JP (1999) Formulating water-resistant TiO_2 sunscreens. Cosmet Toiletries 1999(114):59–63
36. Palmisano G, Augugliaro V, Pagliaro M, Palmisano L (2007), Photocatalysis: a promising route for 21st century organic chemistry Chem. Commun 3425–3437
37. Mahalakshmi M, Arabindoo B, Palanichamy M, Murugesan V (2007) Photocatalytic degradation of carbofuran using semiconductor oxides. J Hazard Mater 143:240–245
38. Abu Tariq M, Faisal M, Muneer M (2005) Semiconductor-mediated photocatalysed degradation of two selected azo dye derivatives,

amaranth and bismarck brown in aqueous suspension. J Hazard Mater 127:172–179
39. Mohamed OS, Gaber AE-AM, Abdel-Wahab AA (2002) Photocatalytic oxidation of selected aryl alcohols in acetonitrile. J Photochem Photobiol A 148:205–210
40. Sharghi H, Hosseini Sarvari M (2003) TiO_2 catalysed One step Beckmann rearrangement of aldehydes and ketones in solvent free conditions. J Chem Res (S) 176
41. Pasha MA, Manjula K, Jayashankara VP (2006) Titanium dioxide-mediated friedel-crafts acylation of aromatic compounds in solvent-free condition under microwave irradiation. Synth React Inorg Met-Org Chem 36:321–324
42. Kassaee MZ, Masrouri H, Movahedi F, Mohammadi R (2010) Helv Chim Acta 93:261–264
43. Subba Rao K. V, Srinivas B, Prasad A. R, Subrahmanyam M, (2000), A novel one step photocatalytic synthesis of dihydropyrazine from ethylenediamine and propylene glycol, Chem. Commun. 1533–1534
44. Subba Rao KV, Subrahmanyam M (2002) Synthesis of 2-methylpiperazine by photocatalytic reaction in a non-aqueous suspension of semiconductor–zeolite composite catalysts. Photochem Photobiol Sci 1:597–599
45. Subba Rao KV, Subrahmanyam M (2002) A novel one step photocatalytic synthesis of 2-methyl quinoxaline from *o*-phenylenediamine and Propyleneglycol over TiO_2/zeolite mediated system. Chem Lett 31:234–235
46. Lang XJ, Ji HW, Chen CC, Ma WH, Zhao JC (2011) Selective formation of imines by aerobic photocatalytic oxidation of amines on TiO_2. Angew Chem Int Ed 50:3934–3937
47. Jing Z, Wang Y, Wu S (2006) Preparation and gas sensing properties of pure and doped γ-Fe_2O_3 by an anhydrous solvent method. Sensor Actuat B-Chem 113:177–181
48. Gao Y, Bao Y, Beerman M, Yasuhara A, Shindo D, Krishman MK (2004) Superstructures of self-assembled cobalt nanocrystals. Appl Phys Lett 84:3361–3363
49. Gupta AK, Gupta M (2005) Synthesis and surface engineering of iron oxide nanoparticles for biomedical applications. Biomaterials 26: 3995–4021
50. Bora DK, Deb P (2009) Fatty acid binding domain mediated conjugation of ultrafine magnetic nanoparticles with albumin protein. Nanoscale Res Lett 4:138–143
51. Liu Q, Cui Z, Ma Z, Bian S, Song W, Wan L (2007) Nanotechnology 18:385605, 5pp
52. Willard MA, Kurihara LK, Carpenter EE, Calvin S, Harris VG (2004) Chemically prepared magnetic nanoparticles. Int Mater Rev 49:125–170
53. Jovalekic C, Zdujic M, Radakovic A, Mitric M (1995) Mechanomechanical synthesis of NiFe2O4 ferrite. Mater Let 24: 365–368
54. Lee S, Jeong J, Shin S, Kim J, Kim J (2004) Synthesis and characterization of superparamagnetic maghemite nanoparticles prepared by coprecipitation technique. J Magn Magn Mater 282:147–150
55. Rockenberger J, Scher EC, Alivisatos AP (1999) A new nonhydrolytic single-precursor approach to surfactant-capped nanocrystals of transition metal oxides. J Am Chem Soc 121: 11595–11596
56. Hyeon T, Lee SS, Park J, Chung Y, Na HB (2001) Synthesis of highly crystalline and monodisperse maghemite nanocrystallites without a size-selection process. J Am Chem Soc 123:12798–12801
57. Souza FL, Lopes KP, Nascente PP, Leite ER (2009) Nanostructured hematite thin films produced by spin-coating deposition solution: application in water splitting. Sol Energ Mat Sol C 93:362–368
58. Sartoretti CJ, Alexander BD, Solarska R, Rutokowska IA, Augustynski J, Cerny R (2005) Photoelectrochemical oxidation of water at transparent ferric oxide film electrodes. J Phys Chem B 109: 13685–13692
59. Hunter GK, O'Young J, Grohe B, Karttunen M, Goldberg HA (2010) The flexible polyelectrolyte hypothesis of protein-biomineral interaction. Langmuir 26:18639–18646
60. Selvan ST, Tan TTY, Yi DK, Jana NR (2010) Functional and multifunctional nanoparticles for bioimaging and biosensing. Langmuir 26:11631–11641
61. Hu XL, Li GS, Yu JC (2010) Design, fabrication and modification of nanostructured materials for environmental and energy applications. Langmuir 26:3031–3039
62. Cooperstein AM, Canavan EH (2010) Biological cell detachment from poly (N-isopropyl acrylamide) and its applications. Langmuir 26:7695–7707
63. Sacher E (2010) Asymmetries in transition metal XPS spectra: metal nanoparticle structure, and interaction with the graphene-structured substrate surface. Langmuir 26:3807–3814
64. Kathiravan A, Renganathan R (2008) An investigation on electron transfer quenching of zinc(II) meso-tetraphenylporphyrin (ZnTPP) by colloidal TiO_2. Spectrochim Acta A 71:1106–1109
65. Kathiravan A, Anbazhagan V, Asha Jhonsi M, Renganathan R (2008) Fluorescence quenching of meso-tetrakis (4-sulfonatophenyl) porphyrins by colloidal TiO_2. Spectrochim Acta A 70:615–618
66. Kathiravan A, Renganathan R (2009) Photoinduced interactions between colloidal TiO_2 nanoparticles and calf thymus-DNA. Polyhedron 28:1374–1378
67. Kathiravan A, Renganathan R (2009) Effect of anchoring group on the photosensitization of colloidal TiO_2 nanoparticles with porphyrins. J Colloid Interface Sci 331:401–407
68. Asha Jhonsi M, Kathiravan A, Renganathan R (2009) An investigation on fluorescence quenching of certain porphyrins by colloidal CdS. J Lumin 129:854–860
69. Kathiravan A, Renganathan R (2009) Photosensitization of colloidal TiO_2 nanoparticles with phycocyanin pigment. J Colloid Interface Sci 335:196–202
70. Asha Jhonsi M, Kathiravan A, Renganathan R (2009) Spectroscopic studies on the interaction of colloidal capped CdS nanoparticles with bovine serum albumin. Colloids Surf B 72:167–172
71. Asha Jhonsi M, Kathiravan A, Renganathan R (2009) Photoinduced interaction between xanthenes dyes and colloidal CdS nanoparticles. J Mol Struct 921:279–284
72. Jayabharathi J, Thanikachalam V, Saravanan K (2009) Effect of substituents on the photoluminescence performance of Ir (III) complexes: Synthesis, electrochemistry and photophysical properties. J Photochem Photobiol A 208:13–20
73. Jayabharathi J, Thanikachalam V, Venkatesh Perumal M, Srinivasan N (2011) Fluorescence resonance energy transfer from a bio-active imidazole derivative 2-(1-phenyl-1H-imidazo [4,5-f] [1,10] phenanthrolin-2-yl)phenol to a bioactive indoloquinolizine system. Spectrochim Acta, Part A 79:236–244
74. Okada S, Okinaka K, Iwawaki H, Furugori M, Hashimoto M, Mukaide T, Kamatani J, Igawa S, Tsuboyama A, Takiguchi T, Ueno K (2005) Substituent effects of iridium complexes for highly efficient red OLEDs. Dalton Trans 9:1583–1590
75. Frisch MJ, Trucks GW, Schlegel HB, Scuseria GE, Robb MA, Cheeseman JR, Montgomery JA Jr, Vreven T, Kudin KN, Burant JC, Millam JM, Iyengar SS, Tomasi J, Barone V, Mennucci B, Cossi M, Scalmani G, Rega N, Petersson GA, Nakatsuji H, Hada M, Ehara M, Toyota K, Fukuda R, Hasegawa J, Ishida M, Nakajima T, Honda Y, Kitao O, Nakai H, Klene M, Li X, Knox JE, Hratchian HP, Cross JB, Bakken V, Adamo C, Jaramillo J, Gomperts R, Stratmann RE, Yazyev O, Austin AJ, Cammi R, Pomelli C, Ochterski JW, Ayala PY, Morokuma K, Voth GA, Salvador P, Dannenberg JJ, Zakrzewski VG, Dapprich S, Daniels AD, Strain MC, Farkas O, Malick DK, Rabuck AD, Raghavachari K, Foresman JB, Ortiz JV, Cui Q, Baboul AG, Clifford S, Cioslowski J, Stefanov BB, Liu G, Liashenko A, Piskorz P, Komaromi I, Martin RL, Fox DJ, Keith T, Al-Laham MA, Peng CY, Nanayakkara A, Challacombe M, Gill PMW, Johnson B, Chen

W, Wong MW, Gonzalez C, Pople JA (2004) Gaussian 03 (Revision E.01). Gaussian, Inc, Wallingford
76. Zhou Z, Qian S, Yao S, Zhang Z (2002) Electron transfer in colloidal TiO_2 semiconductors sensitized by hypocrellin A. Radiat Phys Chem 65:241–248
77. Shin EJ, Kim D (2002) Substituent effect on the fluorescence quenching of various tetraphenylporphyrins by ruthenium tris (2,2′-bipyridine) complex. J Photochem Photobiol A Chem 152:25–31
78. Murov SL, Carmichael I, Hug GL (1993) Handbook of photochemistry, 2nd edn. M. Dekker, Inc., New York, pp 269–273
79. Lin B, Fu Z, Jia Y (2001) Green luminescent center in undoped zinc oxide films deposited on silicon substrates. Appl Phy Lett 79: 943–948
80. Jayabharathi J, Thanikachalam V, Saravanan K (2009) Effect of substituents on the photoluminescence performance of Ir (III) complexes: synthesis, electrochemistry and photophysical properties. J Photochem Photobiol A Chem 208:13–20
81. Cyril L, Earl JK, Sperry WM (1961) Biochemists handbook. E & F.N. Spon, London
82. Chen G.Z, Huang X.Z, Xu J.G, Wang Z.B, Zhang Z.Z, (1990), Method of fluorescent analysis, second ed., Science Press, Beijing, 126, p. 123, (Chapter 4)
83. He WY, Li Y, Xue CX, Hu ZD, Chen XG, Sheng FL (2005) Effect of Chinese medicine alpinetin on the structure of human serum albumin. Bioorg Med Chem 13:1837–1845
84. Hu YJ, Liu Y, Zhang LX (2005) Studies of interaction between colchicine and bovine serum albumin by fluorescence quenching method. J Mol Struct 750:174–178
85. Kavarnos GJ, Turro NJ (1986) Photosensitization by reversible electron transfer: theories, experimental evidence and examples. Chem Rev 86:401–449
86. Parret S, Savary FM, Fouassier JP, Ramamurthy P (1994) Spin-orbit-coupling-induced triplet formation of triphenylpyrylium ion: a flash photolysis study. J Photochem Photobiol A Chem 83:205–209
87. Kikuchi K, Niwa T, Takahashi Y, Ikeda H, Miyashi T (1993) Quenching mechanism in a highly exothermic region of the Rehm-Weller relationship for electron-transfer fluorescence quenching. J Phys Chem 97:5070–5073